Magnetic Moment and Anisotropy of Individual Co Atoms on Graphene

F. Donati,[1] Q. Dubout,[1] G. Autès,[2] F. Patthey,[1] F. Calleja,[1,3] P. Gambardella,[1,4,5] O. V. Yazyev,[2] and H. Brune[1,*]

[1]*Institute of Condensed Matter Physics (ICMP), Ecole Polytechnique Fédérale de Lausanne (EPFL), Station 3, CH-1015, Switzerland*
[2]*Institute of Theoretical Physics, Ecole Polytechnique Fédérale de Lausanne (EPFL), CH-1015 Lausanne, Switzerland*
[3]*Madrid Institute for Advanced Studies, IMDEA Nanoscience, Calle Faraday 9, Campus Cantoblanco, E-28049 Madrid, Spain*
[4]*Catalan Institute of Nanoscience and Nanotechnology (ICN2), UAB Campus, E-08193 Barcelona, Spain*
[5]*Department of Materials, ETH Zurich, CH-8093 Zurich, Switzerland*

(Received 14 August 2013; published 3 December 2013)

We report on the magnetic properties of single Co atoms on graphene on Pt(111). By means of scanning tunneling microscopy spin-excitation spectroscopy, we infer a magnetic anisotropy of $K = -8.1$ meV with out-of-plane hard axis and a magnetic moment of $2.2\mu_B$. Co adsorbs on the sixfold graphene hollow site. Upon hydrogen adsorption, three differently hydrogenated species are identified. Their magnetic properties are very different from those of clean Co. *Ab initio* calculations support our results and reveal that the large magnetic anisotropy stems from strong ligand field effects due to the interaction between Co and graphene orbitals.

DOI: 10.1103/PhysRevLett.111.236801 PACS numbers: 73.22.Pr, 32.10.Dk, 75.30.Gw, 75.70.Rf

Graphene is a promising material for spintronics due to the possibility of realizing controllable spin transport [1], its perfect spin filtering [2], and spin-relaxation lengths of several micrometers at room temperature [3]. Doping graphene by magnetic impurities opens further possibilities [4–6]. In particular, the creation of extended magnetic phases [7], quantum critical Kondo anomalies [8,9], and the strong scattering of spin currents [10] have been predicted. Moreover, for $3d$ metal atoms on graphene, the calculated uniaxial magnetic anisotropies [11,12] are beyond the current record value for a surface-adsorbed atom [13]. Furthermore, hydrogen adsorption has been predicted to change the spin of the adatoms [14], underlining its potential to tailor the magnetic properties. However, the predicted anisotropies and moments are highly controversial and largely depend on how electron correlations are treated. For the prototypical system of Co atoms on graphene, spin moments between 1 and $3\mu_B$ and anisotropies of different signs have been calculated [12,15–17]. At present, there is only one experiment addressing the magnetic properties of transition-metal adatoms on graphene. It reports on-top adsorption, a high-spin ground state, and weak magnetic anisotropy for Co/graphene/SiC(0001) [18].

Here we present the first local measurement of the magnetic moment and anisotropy of individual Co atoms on graphene on Pt(111). This substrate was chosen since graphene binds very weakly to it [19], thus approaching freestanding graphene. Using scanning tunneling microscopy (STM) spin-excitation spectroscopy [20], we find an exceptionally large magnetic anisotropy of $K = -8.1 \pm 0.4$ meV with out-of-plane hard axis and a magnetic moment of $2.2 \pm 0.4\ \mu_B$. Fully relativistic density functional theory (DFT) calculations show the anisotropy to be mainly a hybridization effect. In addition to clean Co, we identify three hydrogenated species, CoH_n, $n \in \{1, 2, 3\}$, with very different magnetic behavior. The coexistence of clean and hydrogenated adatoms is expected to be a general feature of transition metal atoms on graphene that has to be considered in the interpretation of any ensemble measurement.

The experiments were performed with a homebuilt STM operating at $T = 0.4$ K and in magnetic fields up to $B = 8.5$ T perpendicular to the surface. Pt(111) was prepared by means of Ar^+ sputtering and flash annealing (1400 K) cycles until surface impurity concentrations $<0.5\%$ were reached. Graphene patches of various sizes (50–500 nm) were grown by both C segregation (1500 K, 1–3 min) and chemical vapor deposition (10 L C_2H_4 at 1230 K). $5.0 \pm 0.5 \times 10^{-3}$ monolayers of Co were deposited *in situ* at 16 K and $p_{\mathrm{tot}} \leq 8 \times 10^{-10}$ mbar using an e-beam evaporator with a 99.995% purity Co rod. This led to individual immobile adatoms [21]. Constant-current STM images were acquired with a W tip at tunnel current I_t and sample bias V_t given in the figure captions. dI/dV spectra were recorded with open feedback and lock-in using the indicated peak-to-peak modulation voltage V_{mod} at frequency f. d^2I/dV^2 spectra were obtained by numerical differentiation.

The first-principles DFT calculations used the local density approximation with a mean-field Hubbard correction (LDA + U) [22,23], as implemented in QUANTUM-ESPRESSO [24]. We chose $U = 4$ eV for Co in agreement with previous calculations [15]. Spin-orbit effects were accounted for by using the fully relativistic norm-conserving pseudopotentials acting on valence electron wave functions represented in the two-component spinor form [25]. The CoH_n, $n \in \{0, 1, 2, 3\}$, adsorption complexes were placed in a (4×4) supercell of graphene and the structures were fully relaxed. The magnetic anisotropy energy was obtained from the difference of total energies of the out-of-plane and

in-plane spin configurations. The first-principles simulated STM images show the tunnel current at a constant height of $z = 4$ Å above the Co adatom and use the Tersoff-Hamann approximation [26]. The atomic spin and orbital moments, as well as the electronic configuration of the Co adatom, were obtained by projecting the wave functions of the total system onto atomic orbitals of the Co atom.

Figure 1(a) shows an atomically resolved image of the graphene layer. It appears as a hexagonal lattice of protrusions, one per graphene unit cell [27,28]. This can be rationalized by the very small difference in substrate binding energy of the two C atoms in the graphene unit cell. Hence, the contrast is dominated by the difference between C_6 rings and sixfold hollow sites. The latter are imaged as protrusions with the present tip and tunnel parameters. In addition, one distinguishes the graphene moiré pattern caused by the misfit with the Pt(111) substrate [27,29,30]. Graphene on Pt(111) exhibits a variety of moiré structures [27,30]. The results presented here were obtained on the one with a period of (4×4) graphene unit cells; however, they are characteristic of Co adatoms also on the other moiré structures.

A STM image of three Co monomers adsorbed on graphene is shown in Fig. 1(b). The adatoms appear as 2.4 Å high protrusions. The long-range corrugation of the moiré pattern is also visible. A close-up of one Co adatom is shown together with the atomically resolved graphene lattice in Fig. 1(c). From the extrapolation of the graphene lattice close to the adsorbate, we conclude that its apex is located on the sixfold hollow site. This adsorption site corresponds to the lowest energy configuration in our calculations, and the simulated STM image shown in the inset agrees very well with the experiment. The lateral extent of the adsorbate on graphene is, after taking the different apparent height into account, identical to the one on Pt(111), as shown in Fig. 1(d). Therefore, the adsorbate and the electron charge are very well localized. The same adsorption site was also reported for Co atoms on H-intercalated graphene/SiC(0001) [31]. For that system, hollow and top site adsorption coexist, while only top site was observed for graphene/SiC(0001) [18].

After evaporating Co onto graphene, we distinguish four Co-related adsorption species by their apparent heights and inelastic conductance steps, as shown in Figs. 2(a)–2(c). We label them *A*, *B*, *C*, and *D*, in order of increasing abundance on a freshly prepared sample. The differential conductance features of *B* and *C* show no Zeeman splitting in an external field [32] and are therefore very likely of vibrational origin, very similar to the ones reported for Co/graphene/SiO_2/Si(100) [5] and for hydrogenated transition metal and rare earth atoms on Ag(100), where they have been attributed to frustrated translations [33]. In contrast, and as we will see in detail below, the conductance steps characterizing adsorbates *A* and *D* show a clear Zeeman splitting proving their magnetic origin [20].

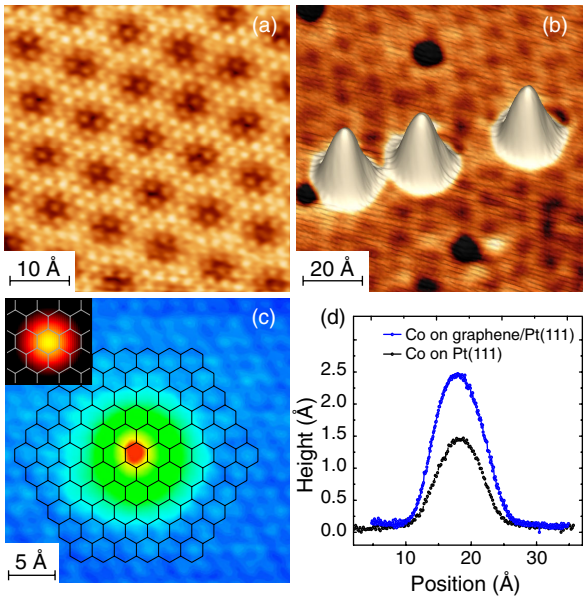

FIG. 1 (color online). (a) STM image of graphene/Pt(111) showing atomic contrast together with moiré pattern ($V_t = -1$ mV, $I_t = 8$ nA, $T = 4.5$ K). (b) STM image of three Co adatoms ($V_t = -20$ mV, $I_t = 1$ nA, $T = 1.7$ K). (c) Hollow adsorption site inferred from adsorbate apex with respect to atomically resolved C lattice sketched in black ($V_t = -50$ mV, $I_t = 100$ pA, $T = 4.5$ K). Inset: Simulated STM image. (d) Line profile of Co atom on graphene/Pt(111) (blue dots, FWHM = 9.0 Å) and on Pt(111) (black dots, FWHM = 8.3 Å) taken with the same tip ($V_t = -100$ mV, $I_t = 100$ pA, $T = 4.5$ K).

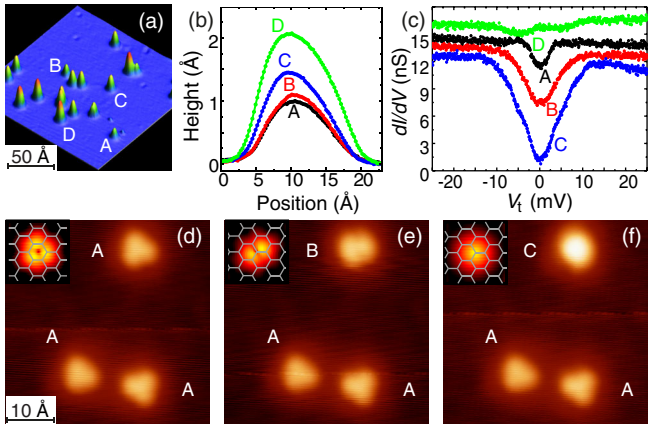

FIG. 2 (color online). (a),(b) Distinct apparent heights for clean Co (*D*), CoH (*C*), CoH_2 (*B*), and CoH_3 (*A*) ($V_t = -25$ mV, $I_t = 50$ pA, $T = 4.5$ K). (c) Characteristic inelastic conductance steps of the four species (feedback gated at $V_t = -25$ mV and $I_t = 250$ pA, $V_{\mathrm{mod}} = 1$ mV, $f = 611$ Hz, $T = 4.5$ K). *A*, *B*, and *D* spectra are offset for clarity. (d) Three CoH_3 complexes imaged as triangles. (e),(f) Successive dehydrogenation of the upper one by voltage pulses ($V_t = -100$ mV, $I_t = 50$ pA, $T = 0.4$ K). Insets: Simulated STM images of the corresponding CoH_n complexes.

In order to identify the four species, we note that adsorption complex A can be transformed into B by applying a tunnel voltage of $|V_t| = 155 \pm 11$ mV with the tip positioned above the adsorbate. This transformation can be continued towards type C with $|V_t| = 180 \pm 7$ mV, and this type is finally converted into type D with $|V_t| = 454 \pm 31$ mV [32]. Further increase of the tunnel voltage leads to a jump of the adsorbate to another hollow site, without altering its type D character. The irreversibility of this transformation suggests a successive chemical modification of the adsorbed species that is terminated once type D is reached.

Individual adsorbed transition metal atoms have been proven to dissociate H_2 with very high efficiency [34]. We observe that direct exposure of the sample to H_2 transforms all species almost entirely into type A. Similarly, exposure to the residual gas of the UHV chamber surrounding the cryostat augments the abundance of A while D strongly decreases [32]. This identifies type A as most and type D as least hydrogenated one. A comparison of high-resolution STM images with simulated ones identifies the intermediate species. Figure 2(d) shows that type A has a triangular envelope in striking agreement with the simulated STM image of CoH_3 shown in the inset. The upper adsorbate in Figs. 2(d)–2(f) has successively been transformed with voltage pulses as described above, while the lower two adsorbates remained unchanged in nature and appearance, proving that the tip apex did not change. Type B is imaged as two distinct protrusions, while C is imaged as a single one, both in excellent agreement with the simulated STM images for CoH_2 and CoH; see insets. Altogether, these observations unequivocally identify species D as clean Co and C, B, A as CoH_n, $n \in \{1, 2, 3\}$. The three adsorbates in Fig. 1(b) are of type D; i.e., they are clean Co adatoms.

We now focus on the magnetic properties of the clean species. Their differential conductance shown in Fig. 3(a) is dominated by two steps at ± 8.1 mV. The step width at $B = 0$ T is with $\Delta E = 950 \pm 350$ μeV, after correction for modulation and T broadening, comparable to reported values for single atoms on metal surfaces [35]. The smaller features visible at -0.5 and 2.5 meV are not reproducible with different tips and therefore stem from the tip. The two steps progressively split in increasing out-of-plane magnetic fields, which is best seen in the d^2I/dV^2 spectra shown in Fig. 3(b).

The field dependence of the step energies E_{step} is presented in Fig. 3(c). The single step splits into two with equal amplitude [see Fig. 3(b)], implying a transition between a singlet ground state ($m = 0$) and a doublet excited state ($m = \pm 1$), and thus an integer value for S [see Fig. 3(d)]. As a general tendency, the occupation of the Co d states increases upon adsorption on a conducting substrate and values of $S \leq 3/2$ are normally observed [36]. Therefore, $S = 1$ is the most reasonable spin multiplicity accounting for our findings. This value is supported by our first-principles calculations [see Fig. 3(e)] and consistent with other theoretical predictions for Co atoms on graphene [15].

To access the magnetic anisotropy, the field dependence of the step energies has been modeled by the following spin Hamiltonian [37]:

$$\hat{H}_{\text{spin}} = g\mu_B \hat{\mathbf{S}} \cdot \mathbf{B} + D\hat{S}_z^2, \tag{1}$$

where g is the electron Landé factor, $\mathbf{B}$ denotes the external magnetic field, D the uniaxial anisotropy parameter, and $\hat{S}$ the adatom total spin operator [38,39]. The z axis is chosen by convention such as to maximize $|D|$. For the present

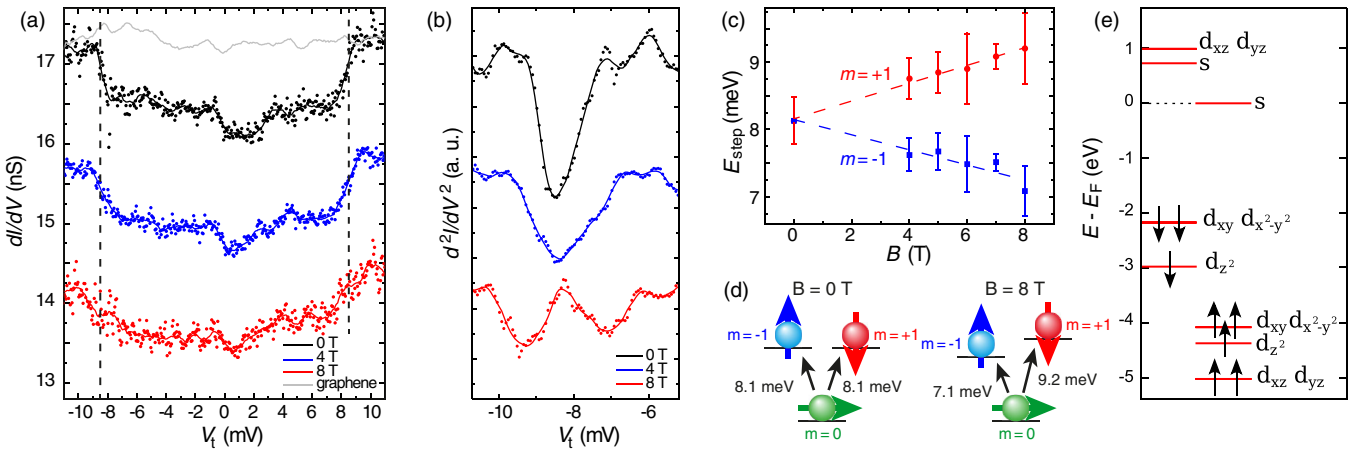

FIG. 3 (color online). (a) Field-dependent dI/dV curves of a clean Co atom proving the magnetic origin of conductance steps at ± 8.1 mV (dots: raw data; lines: smoothened; $V_t = -15$ mV, $I_t = 250$ pA, $V_{\text{mod}} = 200$ μV, $f = 287$ Hz, $T = 0.4$ K). Spectra at 4 and 8 T are offset for clarity. (b) d^2I/dV^2 of left-hand conductance step in (a) showing its Zeeman splitting. (c) Field-dependent spin-excitation energies averaged over 26 adatoms (error bars show standard deviation). (d) An external out-of-plane field lifts the excited state degeneracy leading to the observed Zeeman splitting of the spin-excitation energies. (e) DFT-calculated spin-dependent energies and filling of Co $3d$ and $4s$ levels in the ligand field of graphene.

case, we find that z is the out-of-plane direction. The singlet $m = 0$ ground state implies a positive value of D, and thus a hard out-of-plane axis. Fitting the field-dependent excitation energies of Fig. 3(c), we obtain $D = 8.1 \pm 0.4$ meV and $g = 2.2 \pm 0.4$. Deviations from the free-electron g factor of 2 can be rationalized in terms of orbital contributions to the total magnetic moment, which can be significant for single adatoms [36]. Assuming $S = 1$, we then obtain an effective spin magnetic moment of $2.2 \pm 0.4\mu_B$ and a magnetic anisotropy $K = -DS_z^2 = -8.1 \pm 0.4$ meV [40], with the sign convention that positive values of K signify easy out-of-plane magnetization axes.

For Co on freestanding graphene, our LDA + U calculations show an out-of-plane hard axis, an anisotropy value of $K = -9.55$ meV, and a local spin moment of $m_S = 1.84\mu_B$, all three in excellent agreement with our experimental findings and with one of the three possible scenarios formerly found by DFT [15]. The local orbital moment is predicted to have a strong anisotropy with $m_L^{\parallel} = 0.70\mu_B$ for the in-plane and $m_L^{\perp} = 0.02\mu_B$ for the out-of-plane magnetization. Our calculations further show that the effect of the Pt(111) substrate on the magnetic properties of Co adatoms is very weak [32].

The absolute value of the anisotropy is within the error bar identical to the present single atom record of $K = 9.3 \pm 1.6$ meV measured for Co/Pt(111), where the anisotropy is mostly caused by the spin-orbit coupling of the heavy substrate atoms [13]. Since the spin-orbit coupling is very weak in graphene, the observed anisotropy is surprisingly high. Our calculations reveal that such a high value of K originates from the very strong anisotropy of the orbital moment [41]. Its calculated value $m_L^{\parallel} - m_L^{\perp} = 0.68\mu_B$ is significantly larger than in the case of Co adatoms on Pt(111) [13]. The orbital anisotropy is mostly an effect of the strong hybridization between Co and graphene states and stems from the almost pure axial symmetry of the sixfold adsorption site, which induces a large zero-field splitting of the lowest Co states [15]. Evidence for strong hybridization between Co and graphene is inferred from Co-thin-film–graphene interface anisotropies [42,43] and from the induced magnetization found in Co-island–graphene interfaces [44].

We finally investigated the magnetic properties of CoH_3, which is the only hydrogenated complex displaying spin excitations. Its conductance steps are with 30% relative height much more pronounced than the ones of clean Co with only 3% step height. Therefore, their field splitting is evident already from the dI/dV raw data shown in Fig. 4(a). The striking similarities with the magnetic behavior of clean Co atoms [see Figs. 4(b) and 4(c)] allow us to perform the same analysis as above, obtaining $D = 1.70 \pm 0.05$ meV and $g = 2.19 \pm 0.13$.

For Ni atoms on graphene, hydrogenation has been calculated to transform the nonmagnetic into a magnetic ground state [14]. Here, we observe that the magnetic features of clean Co reappear after the adsorption of three hydrogen atoms, with identical hard axis direction, however, with significantly reduced anisotropy parameter. Since H adsorption can be made reversible by STM manipulation, one can switch between the two anisotropy values in a controlled way. However, the high reactivity of Co atoms on graphene with H_2 complicates the characterization of this system with spatially integrating techniques, such as x-ray magnetic circular dichroism. We note that x-ray magnetic circular dichroism measurements reported for Co atoms on graphene/SiC(0001) have shown very weak magnetic anisotropy, without giving access to the magnetic moment and anisotropy values [18].

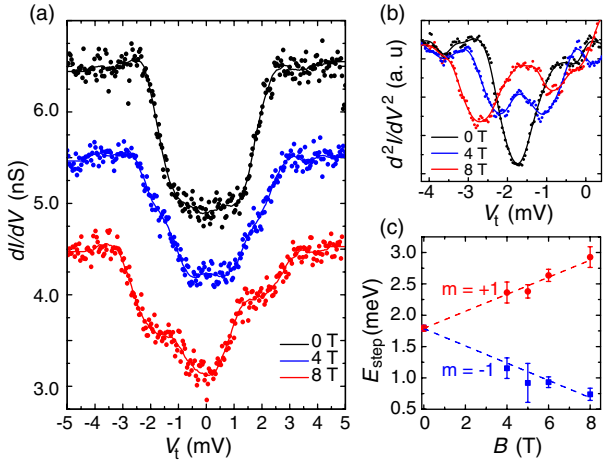

FIG. 4 (color online). (a) Field-induced splitting of the conductance steps of a CoH_3 complex ($V_t = -20$ mV, $I_t = 100$ pA, $V_{mod} = 200$ μV, $f = 611$ Hz, $T = 0.4$ K). Spectra at 4 and 8 T are offset for clarity. (b) Numerical derivative of the negative bias part of (a) showing each step as a minimum. Zero-field width $\Delta E = 700 \pm 100$ μeV. (c) Zeeman splitting of spin-excitation energies averaged over 15 CoH_3 (error bars show standard deviation).

In conclusion, we experimentally determined the adsorption site, magnetic ground state, and anisotropy of single Co atoms on graphene. The adsorption on the sixfold hollow site induces an unprecedentedly high anisotropy for a substrate with small spin-orbit coupling, thus rendering magnetic impurities on graphene very promising candidates for quantum magnetism and spintronics.

We acknowledge L. Claude, A. Lehnert, and M. Etzkorn for their participation in the construction of the microscope. We further acknowledge funding from the Swiss NSF under Grants No. 200020_138043, No. 200020_140479, and No. PP00P2_133552. First-principles computations have been performed at the Swiss National Supercomputing Centre (CSCS) under Project No. s443. We are grateful to A. A. Khajetoorians for his fruitful comments on this manuscript. F. D. and Q. D. contributed equally to this work.

*To whom all correspondence should be addressed.
harald.brune@eplf.ch

[1] Y. W. Son, M. L. Cohen, and S. G. Louie, Nature (London) **444**, 347 (2006).
[2] V. M. Karpan, G. Giovannetti, P. A. Khomyakov, M. Talanana, A. A. Starikov, M. Zwierzycki, J. vandenBrink, G. Brocks, and P. J. Kelly, Phys. Rev. Lett. **99**, 176602 (2007).
[3] N. Tombros, C. Jozsa, M. Popinciuc, H. T. Jonkman, and B. J. van Wees, Nature (London) **448**, 571 (2007).
[4] A. V. Krasheninnikov, P. O. Lehtinen, A. S. Foster, P. Pyykkö, and R. M. Nieminen, Phys. Rev. Lett. **102**, 126807 (2009).
[5] V. W. Brar, R. Decker, H. M. Solowan, Y. Wang, L. Maserati, K. T. Chan, H. Lee, C. O. Girit, A. Zettl, S. G. Louie, M. L. Cohen, and M. F. Crommie, Nat. Phys. **7**, 43 (2011).
[6] Y. Wang, V. W. Brar, A. V. Shytov, Q. Wu, W. Regan, H. Z. Tsai, A. Zettl, L. S. Levitov, and M. F. Crommie, Nat. Phys. **8**, 653 (2012).
[7] H. Sevinçli, M. Topsakal, E. Durgun, and S. Ciraci, Phys. Rev. B **77**, 195434 (2008).
[8] K. Sengupta and G. Baskaran, Phys. Rev. B **77**, 045417 (2008).
[9] B. Uchoa, T. G. Rappoport, and A. H. Castro Neto, Phys. Rev. Lett. **106**, 016801 (2011).
[10] K. M. McCreary, A. G. Swartz, W. Han, J. Fabian, and R. K. Kawakami, Phys. Rev. Lett. **109**, 186604 (2012).
[11] M. Sargolzaei and F. Gudarzi, J. Appl. Phys. **110**, 064303 (2011).
[12] R. J. Xiao, D. Fritsch, M. D. Kuz'min, K. Koepernik, H. Eschrig, M. Richter, K. Vietze, and G. Seifert, Phys. Rev. Lett. **103**, 187201 (2009).
[13] P. Gambardella, S. Rusponi, M. Veronese, S. S. Dhesi, C. Grazioli, A. Dallmeyer, I. Cabria, R. Zeller, P. H. Dederichs, K. Kern, C. Carbone, and H. Brune, Science **300**, 1130 (2003).
[14] T. O. Wehling, A. I. Lichtenstein, and M. I. Katsnelson, Phys. Rev. B **84**, 235110 (2011).
[15] T. O. Wehling, A. V. Balatsky, M. I. Katsnelson, A. I. Lichtenstein, and A. Rosch, Phys. Rev. B **81**, 115427 (2010).
[16] O. V. Yazyev and A. Pasquarello, Phys. Rev. B **82**, 045407 (2010).
[17] A. N. Rudenko, F. J. Keil, M. I. Katsnelson, and A. I. Lichtenstein, Phys. Rev. B **86**, 075422 (2012).
[18] T. Eelbo, M. Waśniowska, P. Thakur, M. Gyamfi, B. Sachs, T. O. Wehling, S. Forti, U. Starke, C. Tieg, A. I. Lichtenstein, and R. Wiesendanger, Phys. Rev. Lett. **110**, 136804 (2013).
[19] J. Wintterlin and M. L. Bocquet, Surf. Sci. **603**, 1841 (2009).
[20] A. J. Heinrich, J. A. Gupta, C. P. Lutz, and D. M. Eigler, Science **306**, 466 (2004).
[21] H. Brune, Surf. Sci. Rep. **31**, 125 (1998).
[22] V. I. Anisimov, J. Zaanen, and O. K. Andersen, Phys. Rev. B **44**, 943 (1991).
[23] M. Cococcioni and S. de Gironcoli, Phys. Rev. B **71**, 035105 (2005).
[24] P. Giannozzi *et al.*, J. Phys. Condens. Matter **21**, 395502 (2009).
[25] A. Dal Corso and A. Mosca Conte, Phys. Rev. B **71**, 115106 (2005).
[26] J. Tersoff and D. R. Hamann, Phys. Rev. B **31**, 805 (1985).
[27] M. Gao, Y. Pan, L. Huang, H. Hu, L. Z. Zhang, H. M. Guo, S. X. Du, and H. J. Gao, Appl. Phys. Lett. **98**, 033101 (2011).
[28] M. Papagno, D. Pacilé, D. Topwal, P. Moras, P. M. Sheverdyaeva, F. D. Natterer, A. Lehnert, S. Rusponi, Q. Dubout, F. Calleja, E. Frantzeskakis, S. Pons, J. Fujii, I. Vobornik, M. Grioni, C. Carbone, and H. Brune, ACS Nano **6**, 9299 (2012).
[29] T. A. Land, T. Michely, R. J. Behm, J. C. Hemminger, and G. Comsa, Surf. Sci. **264**, 261 (1992).
[30] P. Merino, M. Švec, A. L. Pinardi, G. Otero, and J. A. Martín-Gago, ACS Nano **5**, 5627 (2011).
[31] T. Eelbo, M. Waśniowska, M. Gyamfi, S. Forti, U. Starke, and R. Wiesendanger, Phys. Rev. B **87**, 205443 (2013).
[32] See Supplemental Material at http://link.aps.org/supplemental/10.1103/PhysRevLett.111.236801 for additional information about the identification and the magnetic characterization of differently hydrogenated species, the threshold tunnel voltages for transformation of one species into the other, as well as the DFT calculations of the Co adsorption sites and the influence of the Pt substrate.
[33] M. Pivetta, M. Ternes, F. Patthey, and W. D. Schneider, Phys. Rev. Lett. **99**, 126104 (2007).
[34] F. D. Natterer, F. Patthey, and H. Brune, Surf. Sci. **615**, 80 (2013).
[35] A. A. Khajetoorians, S. Lounis, B. Chilian, A. T. Costa, L. Zhou, D. L. Mills, J. Wiebe, and R. Wiesendanger, Phys. Rev. Lett. **106**, 037205 (2011).
[36] H. Brune and P. Gambardella, Surf. Sci. **603**, 1812 (2009).
[37] A. Abragam and B. Bleaney, *Electron Paramagnetic Resonance of Transition Ions* (Clarendon Press, Oxford, England, 1970).
[38] For the hexagonal symmetry, the first transverse anisotropy term is of sixth order [39]; therefore, it can be omitted in Eq. (1) for $S < 3$.
[39] S. K. Misra, C. P. Poole, and H. A. Farach, Appl. Magn. Reson. **11**, 29 (1996).
[40] For a $m = 0 \rightarrow m = \pm 1$ transition, D corresponds to the zero-field excitation energy and is directly measured, while K depends on the choice of S. Therefore, the value of K inferred for $S = 1$ represents a lower limit for the magnetic anisotropy.
[41] P. Bruno, Phys. Rev. B **39**, 865 (1989).
[42] C. Vo-Van, Z. Kassir-Bodon, H. X. Yang, J. Coraux, J. Vogel, S. Pizzini, P. Bayle-Guillemaud, M. Chshiev, L. Ranno, V. Guisset, P. David, V. Salvador, and O. Fruchart, New J. Phys. **12**, 103040 (2010).
[43] N. Rougemaille, A. T. N'Diaye, J. Coraux, C. Vo-Van, O. Fruchart, and A. K. Schmid, Appl. Phys. Lett. **101**, 142403 (2012).
[44] R. Decker, J. Brede, N. Atodiresei, V. Caciuc, S. Blügel, and R. Wiesendanger, Phys. Rev. B **87**, 041403 (2013).